Nature of the Correlated Insulator States in Twisted Bilayer Graphene

Ming Xie and A. H. MacDonald
Department of Physics, The University of Texas at Austin, Austin, Texas 78712, USA

(Received 10 December 2018; revised manuscript received 1 January 2020; accepted 5 February 2020; published 2 March 2020)

We use self-consistent Hartree-Fock calculations performed in the full π-band Hilbert space to assess the nature of the recently discovered correlated insulator states in magic-angle twisted bilayer graphene (TBG). We find that gaps between the flat conduction and valence bands open at neutrality over a wide range of twist angles, sometimes without breaking the system's valley projected $\mathcal{C}_2\mathcal{T}$ symmetry. Broken spin-valley flavor symmetries then enable gapped states to form not only at neutrality, but also at total moiré band filling $n = \pm p/4$ with integer $p = 1, 2, 3$, when the twist angle is close to the magic value at which the flat bands are most narrow. Because the magic-angle flat band quasiparticles are isolated from remote band quasiparticles only for effective dielectric constants larger than ∼20, the gapped states do not necessarily break $\mathcal{C}_2\mathcal{T}$ symmetry and as a consequence the insulating states at $n = \pm 1/4$ and $n = \pm 3/4$ need not exhibit a quantized anomalous Hall effect.

DOI: 10.1103/PhysRevLett.124.097601

Introduction.—A small relative twist between adjacent graphene layers produces a triangular lattice moiré pattern with a spatial periodicity that is inversely related to twist angle. It was noticed [1,2] some years ago that at a series of magic twist angles θ, the moiré pattern yields very flat low-energy bands that promise strong electronic correlations. This promise has now been realized thanks to recent experimental studies [3–12] of bilayers with accurately controlled twist angles that exhibit interaction-induced insulating ground states at moiré band [2] filling factors $n = \pm p/4$, where $p = -3, \ldots, 3$ is the total charge per moiré unit cell. The insulating states are flanked by superconducting domes [5,7]. This exciting discovery has inspired a flurry of theoretical work [13–38] directed toward achieving a more complete understanding of the insulating states and their superconducting satellites. Previous work on the insulating states has been based mainly on an indirect approach that starts by identifying effective lattice models for the flat moiré bands, and then combines these with generalized Hubbard models to address interaction phenomena. In this Letter we explore a different approach.

At small twist angles the electronic structure of twisted bilayer graphene can be accurately described using a continuum model [2,39] in which single-particle electronic states with a four-level spin and valley internal flavor degree of freedom are approximated by four-component envelope function spinors that specify π-orbital amplitudes on the bilayer's four sublattices. The simplest version of the continuum model [2] adds a spatially periodic interlayer hopping term to isolated layer π-orbital Dirac models. This moiré band Hamiltonian is spin independent, and its projections onto graphene's two valleys are related by time-reversal symmetry. Up to an overall energy scale, its spectrum depends on a single twist-angle dependent parameter $\alpha = w/\hbar v k_\theta$, where $w \approx 110$ meV is an interlayer tunneling amplitude, $v \approx 10^6$ m/s is the Dirac velocity, $k_\theta = 2K \sin(\theta/2)$ is the momentum separation between the Brillouin-zone (BZ) corners in different layers, and K is the single-layer BZ corner momentum magnitude.

The valley-projected moiré flat bands in TBG occur not singly, but in valence-conduction pairs connected by two symmetry-protected linear Dirac band crossings. Importantly the two Dirac points of weakly coupled bilayers carry the same chirality. This property implies [14,40,41] that the moiré flat bands can be described only by tight binding models with at the very least four orbitals per flavor per moiré unit cell. Recent work [42] suggests that faithful descriptions of interaction physics using generalized Hubbard models may require the inclusion of at least eight bands per flavor, limiting the motivation for approximate lattice models.

In this Letter we report on a study of the correlation induced insulator states in magic angle TBG that starts directly from the moiré band continuum model and accounts for the long range of the Coulomb interaction between electrons. Our principle results are summarized in Fig. 1. In this figure the largest values of interaction strength parameter ϵ^{-1} correspond to screening by a surrounding hexagonal boron nitride dielectric only. In practice, interactions are sample dependent and always weakened by nearby gates. We find that gapped states occur at neutrality when the effective fine structure constant $\alpha^* = e^2/\epsilon\hbar v_D^*$ exceeds ∼0.4 for twist angle θ above the magic value, and almost always for twists that are smaller. Here v_D^* is the reduced Dirac velocity of the twisted bilayer that vanishes as the magic angle is approached [2]. We attribute the smaller value of the critical fine structure constant in

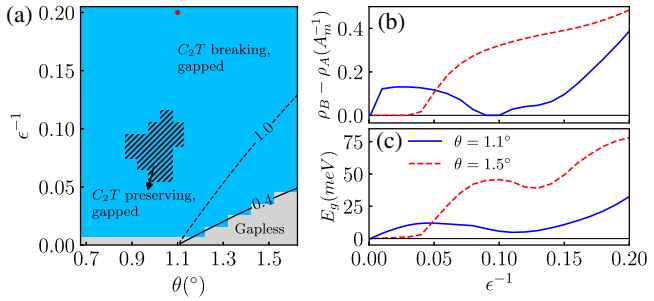

FIG. 1. Phase diagram of neutral bilayers as a function of Coulomb interaction strength, characterized by inverse dielectric constant ϵ^{-1}, and twist angle θ. (a) Insulating states (blue regions) appear for ever weaker interactions as the narrow-band magic angle regime near $\theta \sim 1.1°$ is approached. Above the magic angle, the bilayer's Dirac points are gapped when the effective fine structure constant $\alpha^* = e^2/\epsilon\hbar v_D^*$ exceeds ~0.4 (solid line), where v_D^* is the Dirac velocity of the twisted bilayer,. (v_D^* goes to zero as the magic angle is approached [2].) For $\epsilon^{-1} \gtrsim 0.05$ remote band degrees of freedom play a role in determining the phase diagram details, enabling in particular insulating states that do not break $\mathcal{C}_2\mathcal{T}$ symmetry (hatched region of the phase diagram). (b) $\mathcal{C}_2\mathcal{T}$ -breaking order parameter $\rho_B - \rho_A$ (i.e., sublattice polarization) and (c) global energy gap as a function of interaction strength ϵ^{-1} for $\theta = 1.1°$ (blue solid line) and 1.5° (red dashed line).

twisted bilayer graphene than in the corresponding single-layer graphene [$\alpha^* \sim 1$ [43], indicated as black dashed line in Fig. 1(a)] calculations to the nonuniform spatial distribution of flat band orbitals, which enhances interaction effects. As in single layer graphene [44], these gapped states break $\mathcal{C}_2\mathcal{T}$ symmetry and have nonzero Berry curvatures, whereas the gapless states preserve $\mathcal{C}_2\mathcal{T}$ symmetry. For $n = \pm p/4 \neq 0$, gapped states are enabled by broken flavor symmetries and occur over a much narrower range of twist angles. When the interaction strength is sufficiently strong, gapped states can be opened without breaking the $\mathcal{C}_2\mathcal{T}$ symmetry that protects band crossings when the Hamiltonian is projected onto the strongly correlated flat bands. This property is significant because it has implications for the occurrence of quantized anomalous Hall effects at band filings $n = \pm 1/4$ and $n = \pm 3/4$.

Mean field theory.—Our theoretical approach is guided by the experimental [4] discovery of insulating states in magic angle TBG that are naturally explained by broken symmetries that lift the fourfold spin and valley degeneracy of the band Hamiltonian, and do not require broken translational symmetry. In most cases the ground states of insulators can be described using Hartree-Fock mean-field theory. The difficulty in the TBG case compared to the familiar case of atomic-scale insulators is that the Hamiltonian does not contain strong attractive potential terms within each unit cell that select particular high-weight atomic or ionic configurations. To understand the nature of the insulating states, we must perform unbiased Hartree-Fock calculations in the full [45] π-orbital Hilbert space, placing no restrictions on the flavor or position dependence of the model's four-component envelope function spinors.

A typical self-consistent Hartree-Fock calculation result, for the point $\epsilon = 5$ and $\theta = 1.1°$ marked by a red dot in Fig. 1(a), is summarized in Fig. 2, which illustrates quasiparticle dispersion, topology, and $\mathcal{C}_2\mathcal{T}$ breaking order parameters, and in Table I in which the ground state energies of the noninteracting and interacting cases are partitioned into intralayer and interlayer tunneling and interaction contributions. The technical details of these calculations are described in the Supplemental Material [46]. All energies are expressed relative to the energy of the noninteracting state in the absence of interlayer tunneling, and a neutralizing background charge density is assumed. As shown in Fig. 2, we find separate self-consistent gapped solutions with and without $\mathcal{C}_2\mathcal{T}$ symmetry breaking. The $\mathcal{C}_2\mathcal{T}$ symmetry broken solution features moiré bands with well-defined nonzero Berry curvatures and sublattice polarizations $\rho_B - \rho_A$, and is lowest in energy in most regions of the phase diagram as shown in Fig. 1(a).

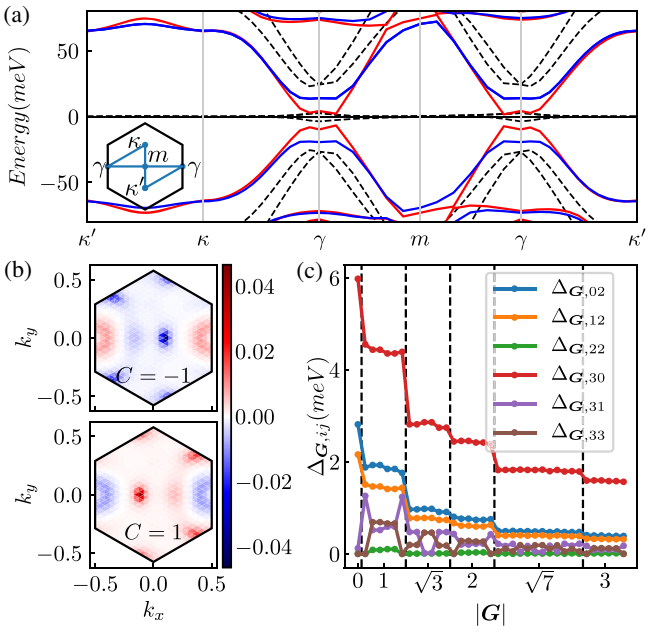

FIG. 2. Properties of quasiparticles at $n = 0$. Only valley K states are shown. (a) Energy dispersion of the $\mathcal{C}_2\mathcal{T}$ breaking (blue) and $\mathcal{C}_2\mathcal{T}$ preserving (red) states at $\theta = 1.1°$ and $\epsilon = 5$. The dotted lines illustrate the noninteracting flat bands. The inset specifies the high symmetry lines in the moiré BZ (mBZ) along which the band energies have been plotted. (b) Berry curvature for lowest conduction band (upper) and the highest valence band (lower) of the broken $\mathcal{C}_2\mathcal{T}$-symmetry solution. Features in these plots are related to avoided crossings between the flat conduction band and higher energy remote conduction bands. (c) Order parameters for $\mathcal{C}_2\mathcal{T}$ symmetry breaking as a function of the reciprocal lattice vector $\boldsymbol{G}$ magnitude. The segments marked by vertical dashed lines group $\boldsymbol{G}$s with the same magnitude.

TABLE I. Total energy per moiré unit cell at neutrality in units of meV calculated in the non-interacting (NI) and self-consistent Hartree-Fock (SCHF) ground states for $\theta = 1.1°$ and $\epsilon = 5$. Gapped insulating states with and without broken $\mathcal{C}_2\mathcal{T}$ compete closely, differing in energy by less than 1 meV per moiré cell. Note that Hartree energies do not play an important role in selecting the broken symmetry state. Both intralayer and interlayer energies grow with the momentum space cut-off, but the difference in energy between non-interacting and interacting states converges.

	Intralayer			Interlayer			
E(meV)	Hopping	Hartree	Fock	Hopping	Hartree	Fock	Total
NI	1417	0	−44	−2636	0	−278	−1541
SCHF	2372	0	−109	−3452	0	−469	−1658

In Table I we note that the ratio of the cost in intralayer tunneling energy, to the energy gain from interlayer tunneling in the noninteracting ground state is 1:2, the ratio that is obtained when interlayer tunneling is treated as a weak perturbation. This observation is consistent with the property [2] that the first magic angle in twisted bilayer graphene is accurately predicted by perturbation theory. Second, we observe that at neutrality both noninteracting and interacting ground states have almost uniform charge density, even though the flat band wave functions are spatially peaked near AA positions in the moiré pattern. The absence of a Hartree energy at neutrality is related to the moiré band Hamiltonian's approximate particle-hole symmetry, and is quite distinct from what would be obtained if the Hilbert space were truncated to include only the lowest energy flat bands. Finally, we note that the condensation energy of the gapped state, which we define as the difference between ground state energy and the expectation value of the Hamiltonian in the noninteracting ground state, is ∼117 meV per moiré period and originates mainly from enhanced interlayer exchange energies. At this value of ϵ^{-1} and θ, total energy minimization including interactions adjusts the ground state so as to enhance interlayer tunneling and interlayer exchange energies at a cost in the intralayer hopping energy, and a substantial part of the ground state rearrangement occurs in higher energy (remote) valence bands. A description of interaction physics in terms of the single-particle flat bands alone is sufficient only for $\epsilon^{-1} \lesssim 0.04$. Even in this case, however, it is necessary to include the Hartree [47] and exchange self-energies from the frozen negative energy sea, which lower the energies of states near the moiré BZ (mBZ) κ and κ' points (see Fig. 2) relative to those near γ, and therefore contributes to quasiparticle band dispersion.

Band topology, insulating states, and broken $\mathcal{C}_2\mathcal{T}$ symmetry.—The moiré band model [2] captures the microscopic tight-binding model's $\mathcal{D}_6$, time reversal $\mathcal{T}$, and $U(1)$ valley symmetries. When the Hamiltonian is projected to a single valley, both $\mathcal{T}$ and $\mathcal{C}_2 = (\mathcal{C}_6)^3$ are lost because they map states between valleys. We are left only with the combined symmetry $\mathcal{C}_2\mathcal{T}$, the threefold rotational symmetry $\mathcal{C}_3$ and a twofold rotation with respect to the x axis $\mathcal{M}_x$. As in monolayer graphene, the $\mathcal{C}_3$ symmetry guarantees Dirac points at both $\boldsymbol{\kappa}$ and $\boldsymbol{\kappa}'$ in the mBZ. We find that near magic angle $\mathcal{C}_3$ is already broken at the weakest interactions we consider and that because of the flatness of the magic-angle bands, the Dirac point positions rapidly move close to γ where the bands are most dispersive. The band topology evolution with θ and ϵ^{-1} is sensitive not only to interactions, but also to the details of the noninteracting band model (see Supplemental Material [46] and [48]). Unless otherwise specified, we have taken $T_{AA}/T_{AB} = 0.8$, where T_{AA} and T_{AB} are the continuum model's intrasublattice and intersublattice hopping parameters, to account for corrugation and strain effects [49]. Even though this choice gives a gap between flat bands and remote bands in the noninteracting limit, near the magic angle a small interaction strength is sufficient to pull the highest valence (lowest conduction) band down (up) in energy to touch the remote bands. The band topology at $\epsilon = 5$ is illustrated in Fig. 2(b) by plotting Berry curvature in the $\mathcal{C}_2\mathcal{T}$ broken state as a function of moiré band momentum. Because of the involvement of remote bands, $\mathcal{C}_2\mathcal{T}$ symmetry no longer guarantees degeneracies between the first conduction and valence bands [14,40]. Breaking $\mathcal{C}_2\mathcal{T}$ symmetry does however lift degeneracies between flat and remote bands, and generates corresponding Berry curvature hot spots that are visible in Fig. 2(b). The difference in condensation energy between $\mathcal{C}_2\mathcal{T}$ breaking and preserving states is extremely small. It follows that near magic twist angles $\mathcal{C}_2\mathcal{T}$ symmetry breaking is not essential for gap formation at moderate interaction strengths.

We characterize states that do break $\mathcal{C}_2\mathcal{T}$ symmetry by performing a Pauli matrix expansion of mBZ averages of the non-local Fock exchange self-energy, defining

$$\frac{A_m}{A}\sum_{\vec{k}}^{mBZ}\langle \boldsymbol{k}+\boldsymbol{G}, l', s'|\Sigma^F|\boldsymbol{k}+\boldsymbol{G}, l, s\rangle = \sum_{ij}\Delta_{\boldsymbol{G},ij}\sigma^i_{s's}\tau^j_{l'l}. \quad (1)$$

where A is the system area, A_m is the moiré unit cell area, $(i, j) = 0, \ldots, 3$ are Pauli matrix labels, $(s's) = A$, B are sublattice labels and $(l'l) = t$, b (top, bottom) are layer labels. (The role of self-energy terms that are off-diagonal in reciprocal lattice vector as $\mathcal{C}_2\mathcal{T}$-breaking order parameters is discussed in the Supplemental Material [46].) The slow fall-off of the order parameter's reciprocal lattice

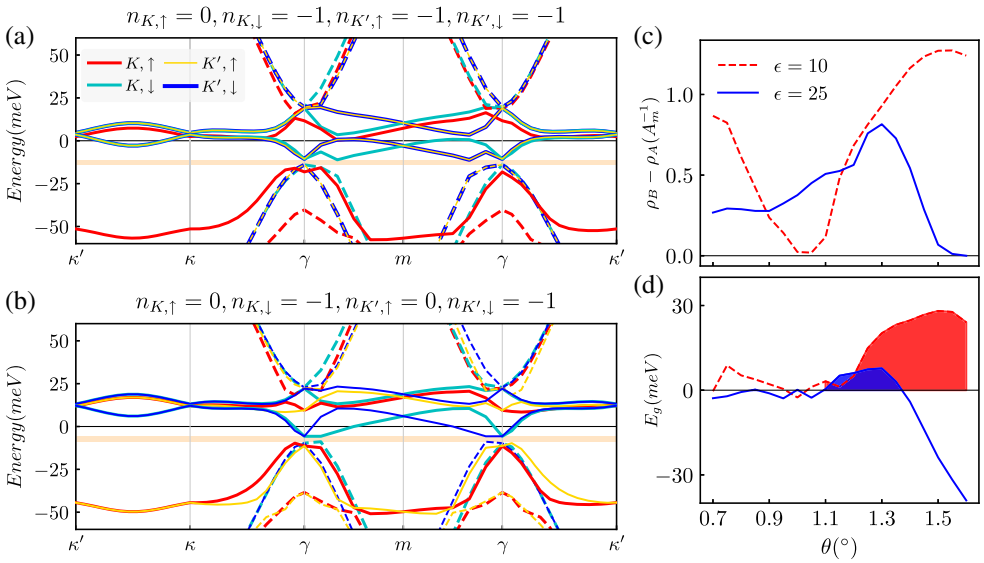

FIG. 3. Quasiparticle dispersion of the SCHF ground states for $\theta = 1.1°$ and $\epsilon = 10$ at filling factors: (a) $n = -3/4$ and (b) $n = -1/2$. The lowest conduction bands and the highest valence bands are plotted as solid lines while remote bands are plotted as dashed lines with flavor-dependent colors. The charge gaps (shaded gold) are $E_g = 2.86$ meV for $n = -3/4$ and $E_g = 3.15$ meV for $n = -1/2$. The flavor dependent band occupation numbers $n_{K/K',\uparrow/\downarrow}$ are measured from neutrality so that 0 means that the corresponding valence band is occupied and -1 means that it is empty. (c) $\mathcal{C}_2\mathcal{T}$ order parameter and (d) global energy gap as a function of twist angle at $n = -1/2$ in a state with one flat valence band occupied for each valley. The red (dashed) and blue (solid) lines correspond to $\epsilon = 10$ and 25, respectively. The flavor polarized insulators are metastable, i.e., the assumed gap is self-consistent, in an interaction strength dependent interval (shaded regions) on the high-twist angle side of the magic angle.

vector expansion in Fig. 2(c) reflects the spatial scale of quasiparticle wave function variation within the moiré unit cell. The largest symmetry-breaking self-energies are proportional to $\sigma^z_{s's}$ and $\tau^0_{l'l}$, i.e., they are layer independent mass terms that favor one sublattice over the other. (We have sought self-consistent solutions with large $\sigma^z_{s's}\tau^z_{l'l}$, self-energies but find that they are not stable.) The Berry curvatures plotted in Fig. 2(b) are large near $\boldsymbol{\gamma}$, not near $\boldsymbol{\kappa}$, $\boldsymbol{\kappa}'$, as they would be if the same self-energy were added to a weakly coupled-layer band Hamiltonian at a larger twist angle. We find that the flat bands sometimes have nonzero Chern numbers [7], implying that quantized anomalous Hall effects can occur [50] when band occupations are valley dependent.

Flavor symmetry breaking.—Because interactions normally induce gaps between conduction and valence bands, which then remain relatively flat, states with flavor dependent band occupancies can be insulating. For example at $n = +p/4$, a state with the first conduction band occupied for p flavors and empty for the remaining flavors is metastable if the exchange-energy shift of the conduction band upon occupation U_X exceeds the conduction band width. A rough estimate based on non-self-consistent Hartree-Fock calculations (see Supplemental Material [46]) yields $U_X \simeq 250$ meV$/\epsilon$, increasing slowly with twist angle. The flat bandwidth, on the other hand, increases rapidly when the magic angle is exceeded, so that insulating states are restricted to the immediate vicinity of the magic angle. Figure 3 illustrates the quasiparticle bands that emerge from a typical fully self-consistent mean-field calculation for a broken flavor symmetry insulator. In mean-field theory, coupling between flavors occurs only through the Hartree potential, which is absent at neutrality and attractive at *AA* sites in the moiré pattern at negative band filling factors. It follows that the energies and wave functions of the Hartree-Fock quasiparticle states of one flavor depend only weakly on the band fillings of the other flavors.

Discussion.—Guided by earlier work [51], we anticipate that there is generally an energetic preference (not captured in continuum models) for states in which opposite valleys are occupied equally. Insulating states at $n = \pm 1/4$ and $\pm 3/4$ must however break valley symmetry and are likely to be maximally valley polarized, which implies quantization of the anomalous Hall effect. It therefore follows from our calculations that quantized anomalous Hall effects in graphene bilayers can occur at quarter band fillings, but that it may not either because $\mathcal{C}_2\mathcal{T}$ symmetry is not broken or because the Chern number happens to equal zero [7]. Indeed there is evidence [7] experimentally that some insulating states at the quarters are Chern insulators and some are not. Further experimental work that maps out how this behavior depends on twist angles and distances to gates will be necessary to make a detailed comparison with mean-filed theory. The important role of thermal and quantum fluctuations of the collective fields present in the insulating states will be discussed elsewhere.

This work was supported by the U.S. Department of Energy, Office of Science, Basic Energy Sciences, under Award No. DE-FG02-02ER45958. We acknowledge helpful interactions with A. Bernevig, D. Efetov, P. Potasz, N. Regnault, T. Senthil, A. Vishwanath, and F. Wu.

Note added.—Recently, three independent related papers [52–54] appeared, which report related results from mean-field theory and are complimentary to this Letter.

[1] E. Suarez Morell, J. D. Correa, P. Vargas, M. Pacheco, and Z. Barticevic, Phys. Rev. B **82**, 121407(R) (2010).
[2] R. Bistritzer and A. H. MacDonald, Proc. Natl. Acad. Sci. U.S.A. **108**, 12233 (2011).
[3] K. Kim, A. DaSilva, S. Huang, B. Fallahazad, S. Larentis, T. Taniguchi, K. Watanabe, B. J. LeRoy, A. H. MacDonald, and E. Tutuc, Proc. Natl. Acad. Sci. U.S.A. **114**, 3364 (2017).
[4] Y. Cao, V. Fatemi, A. Demir, S. Fang, S. L. Tomarken, J. Y. Luo, J. D. Sanchez-Yamagishi, K. Watanabe, T. Taniguchi, E. Kaxiras, R. C. Ashoori, and P. Jarillo-Herrero, Nature (London) **556**, 80 (2018).
[5] Y. Cao, V. Fatemi, S. Fang, K. Watanabe, T. Taniguchi, E. Kaxiras, and P. Jarillo-Herrero, Nature (London) **556**, 43 (2018).
[6] M. Yankowitz, S. Chen, H. Polshyn, K. Watanabe, T. Taniguchi, D. Graf, A. F. Young, and C. R. Dean, Science **363**, 1059 (2019).
[7] X. Lu, P. Stepanov, W. Yang, M. Xie, M. A. Aamir, I. Das, C. Urgell, K. Watanabe, T. Taniguchi, G. Zhang, A. Bachtold, A. H. MacDonald, and D. K. Efetov, Nature (London) **574**, 653 (2019).
[8] A. L. Sharpe, E. J. Fox, A. W. Barnard, J. Finney, K. Watanabe, T. Taniguchi, M. A. Kastner, and D. Goldhaber-Gordon, Science **365**, 605 (2019).
[9] Y. Jiang, X. Lai, K. Watanabe, T. Taniguchi, K. Haule, J. Mao, and Eva Y. Andrei, Nature (London) **573**, 91 (2019).
[10] A. Kerelsky, L. McGilly, D. M. Kennes, L. Xian, M. Yankowitz, S. Chen, K. Watanabe, T. Taniguchi, J. Hone, C. Dean, A. Rubio, and A. N. Pasupathy, Nature (London) **572**, 95 (2019).
[11] Y. Xie, B. Lian, B. Jäck, X. Liu, C.-L. Chiu, K. Watanabe, T. Taniguchi, B. A. Bernevig, and A. Yazdani, Nature (London) **572**, 101 (2019).
[12] M. Serlin, C. L. Tschirhart, H. Polshyn, Y. Zhang, J. Zhu, K. Watanabe, T. Taniguchi, L. Balents, and A. F. Young, arXiv:1907.00261.
[13] N. F. Q. Yuan and L. Fu, Phys. Rev. B **98**, 045103 (2018).
[14] H. C. Po, L. Zou, A. Vishwanath, and T. Senthil, Phys. Rev. X **8**, 031089 (2018).
[15] H. Guo, X. Zhu, S. Feng, and R. T. Scalettar, Phys. Rev. B **97**, 235453 (2018).
[16] B. Padhi, C. Setty, and P. W. Phillips, Nano Lett. **18**, 6175 (2018).
[17] V. Y. Irkhin and Y. N. Skryabin, JETP Lett. **107**, 651 (2018).
[18] J. F. Dodaro, S. A. Kivelson, Y. Schattner, X.-Q. Sun, and C. Wang, Phys. Rev. B **98**, 075154 (2018).
[19] T. Huang, L. Zhang, and T. Ma, Sci. Bull. **64**, 310 (2019).
[20] C.-C. Liu, L.-D. Zhang, W.-Q. Chen, and F. Yang, Phys. Rev. Lett. **121**, 217001 (2018).
[21] X. Y. Xu, K. T. Law, and P. A. Lee, Phys. Rev. B **98**, 121406(R) (2018).
[22] J. Kang and O. Vafek, Phys. Rev. X **8**, 031088 (2018).
[23] L. Rademaker and P. Mellado, Phys. Rev. B **98**, 235158 (2018).
[24] M. Koshino, N. F. Q. Yuan, T. Koretsune, M. Ochi, K. Kuroki, and L. Fu, Phys. Rev. X **8**, 031087(R) (2018).
[25] J. M. Pizarro, M. J. Calderon, and E. Bascones, J. Phys. Commun. **3**, 035024 (2019).
[26] M. Ochi, M. Koshino, and K. Kuroki, Phys. Rev. B **98**, 081102(R) (2018).
[27] H. Isobe, N. F. Q. Yuan, and L. Fu, Phys. Rev. X **8**, 041041 (2018).
[28] A. Thomson, S. Chatterjee, S. Sachdev, and M. S. Scheurer, Phys. Rev. B **98**, 075109 (2018).
[29] C. Xu and L. Balents, Phys. Rev. Lett. **121**, 087001 (2018).
[30] F. Wu, A. H. MacDonald, and I. Martin, Phys. Rev. Lett. **121**, 257001 (2018).
[31] B. Roy and V. Juricic, Phys. Rev. B **99**, 121407(R) (2019).
[32] S. Ray, J. Jung, and T. Das, Phys. Rev. B **99**, 134515 (2019).
[33] T. J. Peltonen, R. Ojajarvi, and T. T. Heikkila, Phys. Rev. B **98**, 220504(R) (2018).
[34] Y.-Z. You and A. Vishwanath, arXiv:1805.06867.
[35] X.-C. Wu, K. A. Pawlak, C.-M. Jian, and C. Xu, arXiv:1805.06906.
[36] M. Fidrysiak, M. Zegrodnik, and J. Spalek, Phys. Rev. B **98**, 085436 (2018).
[37] K. Seo, V. N. Kotov, and B. Uchoa, Phys. Rev. Lett. **122**, 246402 (2019).
[38] J. Kang and O. Vafek, Phys. Rev. Lett. **122**, 246401 (2019).
[39] J. M. B. Lopes dos Santos, N. M. R. Peres, and A. H. Castro Neto, Phys. Rev. Lett. **99**, 256802 (2007).
[40] H. C. Po, H. Watanabe, and A. Vishwanath, Phys. Rev. Lett. **121**, 126402 (2018).
[41] Z. Song, Z. Wang, W. Shi, G. Li, C. Fang, and B. A. Bernevig, Phys. Rev. Lett. **123**, 036401 (2019).
[42] H. C. Po, L. Zou, T. Senthil, and A. Vishwanath, Phys. Rev. B **99**, 195455 (2019).
[43] H. Min, G. Borghi, M. Polini, and A. H. MacDonald, Phys. Rev. B **77**, 041407(R) (2008).
[44] A. H. MacDonald, J. Jung, and F. Zhang, Phys. Scr. **T146**, 014012 (2012).
[45] In the continuum model single-electron states are described by valley-dependent four-component envelope-function spinors that specify position-dependent projections onto π orbitals on each of the bilayer's four sublattices. In the full π-band Hilbert space any dependence on position consistent with the emergent moiré superlattice periodicity is allowed. In practice, we expand the periodic part of the Bloch spinors at each momentum in the moiré Brillouin zone in reciprocal lattice vectors, truncating at convergence.
[46] See Supplemental Material at http://link.aps.org/supplemental/10.1103/PhysRevLett.124.097601 for detailed description of the unbiased Hartree-Fock mean-field theory for twisted bilayer graphene, Fock self-energy

decomposition, and band topology evolution with twist angle and interaction strength. We also present some detailed analysis of flavor symmetry breaking states and non-interacting eigenstates at high symmetry momenta.

[47] F. Guinea and N. R. Walet, Proc. Natl. Acad. Sci. U.S.A. **115**, 13174 (2018).

[48] M. Xie and A. H. MacDonald (to be published).

[49] S. Carr, S. Fang, Z. Zhu, and E. Kaxiras, Phys. Rev. Research **1**, 013001 (2019).

[50] Y.-H. Zhang, D. Mao, Y. Cao, P. Jarillo-Herrero, and T. Senthil, Phys. Rev. B **99**, 075127 (2019).

[51] J. Jung, A. Raoux, Z. Qiao, and A. H. MacDonald, Phys. Rev. B **89**, 205414 (2014).

[52] S. Liu, E. Khalaf, J. Y. Lee, and A. Vishwanath, arXiv:1905.07409.

[53] N. Bultinck, E. Khalaf, S. Liu, S. Chatterjee, A. Vishwanath, and M. P. Zaletel, arXiv:1911.02045.

[54] J. Liu and X. Dai, arXiv:1911.03760.